Journal of
Plant Ecology

VOLUME 12, NUMBER 5,
PAGES 804–814

OCTOBER 2019

doi: 10.1093/jpe/rtz024

Advanced Access published
7 May 2019

available online at
https://academic.oup.com/jpe

Changes in productivity and carbon storage of grasslands in China under future global warming scenarios of 1.5°C and 2°C

Zhaoqi Wang[1], *Jinfeng Chang*[2], *Shushi Peng*[1,*], *Shilong Piao*[1], *Philippe Ciais*[2] *and Richard Betts*[3,4]

[1] *Sino-French Institute for Earth System Science, College of Urban and Environmental Sciences, Peking University, Beijing 100871, China*
[2] *Laboratoire des Sciences du Climat et de l'Environnement, LSCE/IPSL, CEA-CNRS-UVSQ, Université Paris-Saclay, F-91191 Gif-sur-Yvette, France*
[3] *College of Life and Environmental Sciences, University of Exeter, Exeter EX4 4PS, UK*
[4] *Met Office Hadley Centre, Exeter EX1 3PB, UK*
*Corresponding address. College of Urban and Environmental Sciences, Peking University, Beijing 100871, China; E-mail: speng@pku.edu.cn

Abstract

Aims

The impacts of future global warming of 1.5°C and 2°C on the productivity and carbon (C) storage of grasslands in China are not clear yet, although grasslands in China support ~45 million agricultural populations and more than 238 million livestock populations, and are sensitive to global warming.

Methods

This study used a process-based terrestrial ecosystem model named ORCHIDEE to simulate C cycle of alpine meadows and temperate grasslands in China. This model was driven by high-resolution (0.5° × 0.5°) climate of global specific warming levels (SWL) of 1.5°C and 2°C (warmer than pre-industrial level), which is downscaled by EC-EARTH3-HR v3.1 with sea surface temperature and sea-ice concentration as boundary conditions from IPSL-CM5-LR (low spatial resolution, 2.5° × 1.5°) Earth system model (ESM).

Important Findings

Compared with baseline (1971–2005), the mean annual air temperature over Chinese grasslands increased by 2.5°C and 3.7°C under SWL1.5 and SWL2, respectively. The increase in temperature in the alpine meadow was higher than that in the temperate grassland under both SWL1.5 and SWL2. Precipitation was also shown an increasing trend under SWL2 over most of the Chinese grasslands. Strong increases in gross primary productivity (GPP) were simulated in the Chinese grasslands, and the mean annual GPP (GPP_{MA}) increased by 19.32% and 43.62% under SWL1.5 and SWL2, respectively. The C storage increased by 0.64 Pg C and 1.37 Pg C under SWL1.5 and SWL2 for 50 years simulations. The GPP_{MA} was $0.67^{0.88}_{0.39}$ (0.82) (model mean$^{max}_{min}$ (this study)), $0.85^{1.24}_{0.45}$ (0.97) and $0.94^{1.30}_{0.61}$ (1.17) Pg C year^{-1} under baseline, SWL1.5 and SWL2 modeled by four CMIP5 ESMs (phase 5 of the Coupled Model Inter-comparison Project Earth System Models). In contrast, the mean annual net biome productivity was $-18.55^{4.47}_{-40.37}$ (−3.61), $18.65^{64.03}_{-2.03}$ (10.29) and $24.15^{38.77}_{8.38}$ (24.93) Tg C year^{-1} under baseline, SWL1.5 and SWL2 modeled by the four CMIP5 ESMs. Our results indicated that the Chinese grasslands would have higher productivity than the baseline and can mitigate climate change through increased C sequestration under future global warming of 1.5°C and 2°C with the increase of precipitation and the global increase of atmospheric CO_2 concentration.

Keywords: productivity, carbon storage, specific warming level, grassland, climate change

Received: 12 August 2018, Revised: 25 March 2019, Accepted: 6 May 2019

INTRODUCTION

Grasslands account for nearly 20% of the global land surface area (Scurlock *et al.* 1998), and play a crucial role in ecology and food security (Conant *et al.* 2001), climate change (Piao *et al.* 2009a) and the global carbon (C) budget (Piao *et al.* 2009b). Grasslands in China cover approximately 4 million km^2 (nearly 40% of China's land areas; Akiyama and Kawamura 2007; Nan 2005) and provide ecosystem services for a 45 million agricultural population by supporting a 238

million livestock population (National Bureau of Statistics of China 2016). Alpine meadows (AM) and temperate grasslands (TG) are the main grassland types in China, which are mainly located in the Qinghai-Tibet Plateau (QTP) and Inner Mongolia Plateau (IMP). The vegetation in these regions is sensitive to climate change because of its vulnerability and the alpine or dry environment (Chen *et al.* 2013; Jin *et al.* 2000; Wang *et al.* 2016). However, how gross primary productivity (GPP) and net biome productivity (NBP) of the grasslands in China respond to climate change under future global warming remains unclear.

The goal of Paris Agreement is to keep the increase in global mean temperature below 2°C compared with pre-industrial level, with an aspirational target of 1.5°C, because higher levels of global warming would lead to negative impacts on the environment and human society (Xu *et al.* 2017), e.g., the future high-end warming is likely to increase the risk of flooding in European (Alfieri *et al.* 2016). The frequency of extreme El Niño events will also increase along with the rising global mean temperature (Wang *et al.* 2017*a*). The increased drought period was projected in the Mediterranean under global warming of 1.5°C to 2°C (compared with pre-industrial level) (Schleussner *et al.* 2016). The glacier ice, in the high mountains of Asia, will be substantially reduced under future warming (Kraaijenbrink *et al.* 2017), as well as permafrost loss in high latitude of the northern hemisphere (Chadburn *et al.* 2015). Chang *et al.* (2017) reported that the grasslands productivity over Europe will increase with an earlier winter–spring phenology under the scenario of rising CO_2 and warming in the future. However, the impacts of a specified warming level of 1.5°C (SWL (specific warming levels)1.5) and 2°C (SWL2) of future global warming on regional grasslands productivity and C storage are not well understood yet. With launch of the Inter-Sectoral Impact Model Inter-comparison Project (ISIMIP) (https://www.isimip.org/) which aims at the impacts of climate change across affected sectors and spatial scales under different climate change scenario, it is time to investigate and understand the different impacts of global warming levels of 1.5°C and 2°C on the regional productivity and C storage of Chinese grasslands (He *et al.* 2012; Lu *et al.* 2013; Piao *et al.* 2005). This investigation about the impacts of global warming levels of 1.5°C and 2°C on Chinese grasslands can help to understand the responses of grasslands to future global climate change, and also help policymakers for sustainable development of the grasslands in China.

For this purpose, we utilized a process-based ecosystem model ORCHIDEE to simulate the GPP and NBP of Chinese grasslands, and then analyzed the changes in temperature, precipitation, GPP and C storage of AM and TG in China under SWL1.5 and SWL2. Our results are expected to provide predictions for the changes in productivity and C storage of Chinese grasslands in SWLs, and to be helpful for the grasslands management and climate mitigation in China.

METHODS

Model description

ORCHIDEE (the version of rev3623), a process-based terrestrial ecosystem model, was used to simulate the GPP and NBP of Chinese grasslands (Chang *et al.* 2017; Krinner *et al.* 2005; Peng *et al.* 2013; Piao *et al.* 2007a). The ORCHIDEE model can simulate the surface energy balance, hydrological cycle and C cycle processes in offline mode with climate forcing input. Details and equations of ORCHIDEE are described by Krinner *et al.* (2005). The source code for ORCHIDEE rev3623 can be found at http://forge.ipsl.jussieu.fr/orchidee/wiki.

Simulation set-up and data processing

We ran ORCHIDEE over China using the high-resolution (0.5° × 0.5°) climate forcing downscaled by EC-EARTH3-HR v3.1 (Alfieri *et al.* 2017; Hazeleger *et al.* 2012) with sea surface temperature and sea-ice concentration as boundary conditions from IPSL-CM5-LR (low spatial resolution, 2.5° × 1.5°) Earth system model (ESM), yet preserving the original global extent. For the spin-up, ORCHIDEE was forced by cycled climate forcing from 1971 to 1980 with an accelerated module for soil C to reach the equilibrium state. Then a historical simulation for baseline (1971–2005) was continued from the simulated equilibrium state.

SWL here is defined as the global mean temperature reaches a given warming level compared with the pre-industrial period (1881–1910) (following Vautard *et al.* 2014). In this study, SWL1.5 and SWL2 were reached in 2016 and 2031 in the climate simulations of IPSL-CM5-LR ESM under RCP8.5 (more details can be found at https://helixclimate.eu/). For SWL1.5 and SWL2 simulations, a 50-year simulation was performed with climate forcing randomly selected from the 7 years around the year reaching each SWL (2013–2019 for SWL1.5 and 2028–2034 for SWL2) to identify the changes in productivity and C storage of Chinese grasslands. The atmospheric CO_2 concentration was kept at 401.6 ppm and 448.8 ppm in the simulations of SWL1.5 and SWL2, corresponding to the IPSL-CM5-LR levels of prescribed CO_2 when SWL1.5 and SWL2 are reached (Table 1). The simulated daily GPP and NBP were output with a spatial resolution of 0.5° × 0.5°. We further composited the daily data into annual, and the spatial resolution was resampled to 0.1° × 0.1° by using a cubic method. The code used in this study is available from the corresponding author on request.

Table 1: establishment of scenarios for SWLs in this study

Forcing	Scenarios	CO_2 (ppm)	Time
EC-Earth3-HR+ IPSL-CM5-LR	Baseline	326–379	1971–2005
	SWL1.5	402	2016–2065
	SWL2	449	2031–2080

Grasslands map

The grasslands map was extracted from 1:1,000,000 China vegetation map (Yao *et al.* 2018; Zhang 2007). The vector grasslands map was further reclassified into the AM and TG (Fig. 1) based on the sub-type vegetation property. In AM, including alpine *Kobresia* and forb meadow, the dominant species are *Kobersia pygmaea*, *Kobresia humilis*, *Kobresia capillifolia*, *Kobresia setchwanensis*, *Kobresia yunnanensis* and *Kobresia bellardii*. The TG including temperate grass-forb steppe, temperate needlegrass arid steppe, temperate dwarf needlegrass and dwarf semi-shrubby desert steppe, the dominant species are *Stipa baicalensis*, *Stipa grandis*, *Stipa krylovii*, *Stipa bungiana* and *Stipa capillata* (Zhang 2007). The original vector map was converted to raster data with a spatial resolution of 0.1° × 0.1° by using a cubic method.

GPP data from the observation-based model and CMIP5 ESMs

Two observation-based gridded GPP products were used in this study to validate the simulated GPP from ORCHIDEE model: (i) FLUXCOM GPP with a spatial resolution of 0.5° × 0.5° up-scaled from site-level measured GPP from 224 eddy flux towers by three machine learning methods (Random Forests (RF), Artificial Neural Networks (ANN) and Multivariate Adaptive Regression Splines (MARS)) (Jung *et al.* 2017; Tramontana *et al.* 2016; available at https://www.bgc-jena.mpg.de/geodb/projects/Home.php); (ii) MODIS GPP product (MOD17C6) derived from light use efficiency model calibrated with GPP data from eddy flux towers (Running *et al.* 2015). The 8-day MOD17C6 data were further composite to annual GPP.

The CMIP5 (phase 5 of the Coupled Model Inter-comparison Project) ESMs data used in this study included GPP and NBP of four ESMs (GFDL-ESM2M, HadGEM2-ES, IPSL-CM5A-LR and NorESM1-ME) (Taylor *et al.* 2012) in historical (1971 to 2005) and future (2006 to 2100) representative concentration pathway 2.6, 4.5, 6.0 and 8.5 (RCP2.6, RCP4.5, RCP6.0 and RCP8.5, respectively). The mean annual GPP (GPP_{MA}) and NBP (NBP_{MA}) of the four ESMs in baseline and SWLs under RCP8.5 were used to represent GPP and NBP uncertainty. The projected air temperature (2006 to 2100) of the four ESMs under RCP8.5 was used to determine which year of the ESMs reached SWL1.5 or SWL2 (Table 2).

To clarify the difference between SWLs and RCPs, the ΔGPP_{MA} (ΔC storage) of each CMIP5 ESM was calculated as the difference between the GPP_{MA} (sum of NBP_{MA}) of the period 2081–2100 and that of the baseline period (1971–2005). For each CMIP5 ESM, the output of the first realization (r1i1p1) was used in this study. These data are available on https://esgf-node.llnl.gov/projects/cmip5/. All data were resampled to 0.1°× 0.1° by using the cubic method before performing any analysis.

RESULTS

Model validation

The FLUXCOM GPP_{MA} of ANN, MARS and RF was 0.55, 0.70 and 0.93 Pg C $year^{-1}$ from 1980 to 2013. Correspondingly, the GPP_{MA} simulated by our model (0.82 Pg C $year^{-1}$) was higher than the mean GPP_{MA} of the three machine learning methods (0.73 ± 0.16 Pg C $year^{-1}$). The GPP_{MA} of MOD17C6 was 0.59 Pg C $year^{-1}$ from 2001 to 2017, lower than that of our model

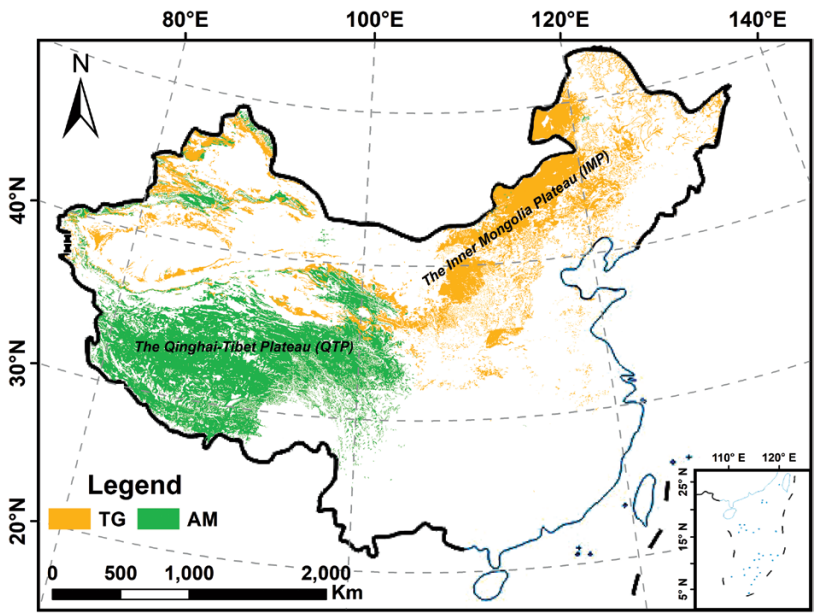

Figure 1: spatial distribution of the grassland types in China. TG, temperate grassland (yellow); AM, alpine meadow (green).

Table 2: the year of each ESM reaching SWL1.5 and SWL2, the 5 years selected were used to get GPP_{MA} and NBP_{MA} of Chinese grasslands for comparison

ESMs	Year of reached SWL1.5	Year of reached SWL2	Years selected for SWL1.5	Years selected for SWL2
GFDL-ESM2M	2036	2051	2034–2038	2049–2053
HadGEM2-ES	2021	2035	2019–2023	2033–2037
IPSL-CM5A-LR	2016	2031	2014–2018	2029–2033
NorESM1-ME	2029	2047	2027–2031	2045–2049

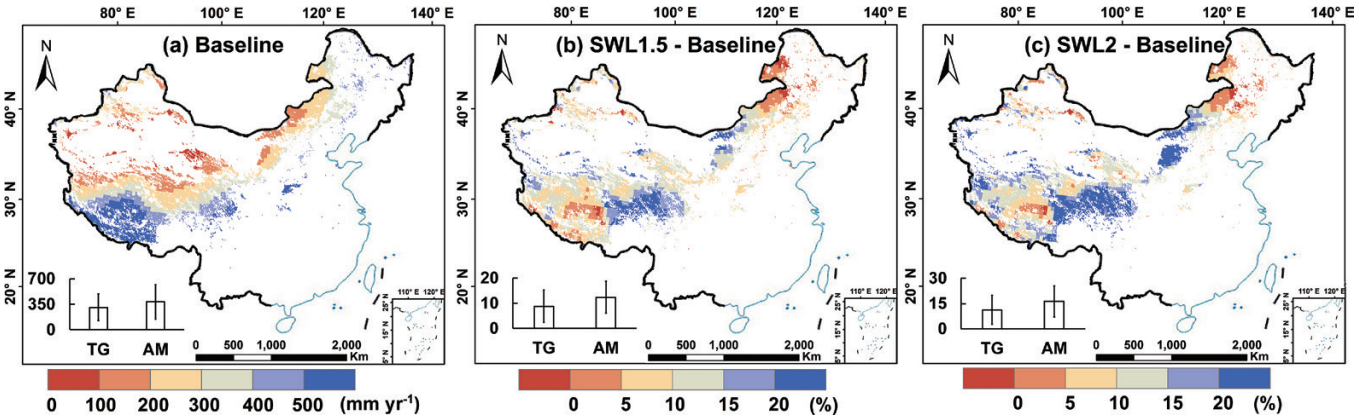

Figure 2: spatial pattern of precipitation in Chinese grasslands under baseline (1971–2005) (**a**) and its relative changes under SWL1.5 (**b**) and SWL2 (**c**). The lower left inset denotes the precipitation changes (%) in temperate grasslands (TG) and alpine meadow (AM).

(0.88 Pg C $year^{-1}$) during the same period. The spatial patterns of GPP_{MA} of ANN, MARS, RF and MOD17C6 were similar to that of ORCHIDEE during the baseline period (online supplementary Fig. S1), but our simulated GPP_{MA} was higher than the observation-based products in the southern Tibetan Plateau because of the higher precipitation in the downscaled climate forcing in this region (Fig. 2a). We also verified that the downscaled climate forcing can generally match the spatial pattern of observed climate from 582 meteorological stations, with outliers in precipitation over southern Tibetan Plateau (online supplementary Fig. S2).

Spatial distribution of climate and climate change under SWLs

Fig. 2a shows the spatial distribution of mean annual precipitation (MAP) during the baseline period. MAP was higher than that of baseline in most of the Chinese grasslands under SWL1.5, especially in the southeastern Qinghai-Tibet Plateau (QTP) where MAP increased more than 20% (Fig. 2b). Only 3.4% of the Chinese grasslands, mainly in the northeastern Inner Mongolia Plateau (IMP), experienced a decreasing trend in MAP under SWL1.5. Under SWL2, 97.4% of the Chinese grasslands exhibited an increasing trend of MAP, especially in the southeastern QTP and the middle-southern IMP where MAP increased by more than 20% (Fig. 2c). In summary, under both SWL1.5 and SWL2, the magnitude of MAP increase in AM was higher than that in TG (low left inset in Fig. 2b and c).

During the baseline period, over 56.7% of the Chinese grasslands have a mean annual temperature (MAT) less than 0°C, which were mainly distributed in the QTP (Fig. 3a). Compared with baseline, the MAT over Chinese grasslands increased by 2.5°C under SWL1.5. The QTP has the highest increases in MAT (Fig. 3b), corresponding to a higher increase in MAT over AM (2.7°C) than that over TG (2.3°C) (low left inset in Fig. 3b). Moreover, the MAT over Chinese grasslands increased by 3.7°C under SWL2 (Fig. 3c), and AM and TG increased by 4.1°C and 3.4°C, respectively (low left inset in Fig. 3c). In summary, compared with baseline, the climate over Chinese grasslands becomes warmer and wetter under SWL1.5 and SWL2.

Changes in GPP under SWL1.5 and SWL2

Strong increases in the GPP of Chinese grasslands were simulated under SWL1.5 and SWL2 compared with baseline (Fig. 4). The GPP_{MA} of Chinese grasslands was estimated to be 0.82 ± 0.09 Pg C $year^{-1}$ during the baseline period, which increased by 0.16 and 0.36 Pg C $year^{-1}$ under SWL1.5 and SWL2, respectively. Compared with baseline, 84.0% of the Chinese grasslands experienced significant increases in GPP_{MA} under SWL1.5 (Fig. 4a), with the most substantial increase over AM. However, the GPP_{MA} in northeastern China, where TG is the dominated grasslands type, was modeled to decrease under SWL1.5. The increase in GPP_{MA} of AM reached 0.15 Pg C $year^{-1}$, while a smaller increase in GPP_{MA} was found over TG (0.01 Pg C $year^{-1}$) with the decrease in GPP_{MA} over the northeastern IMP (lower left inset in Fig. 4a).

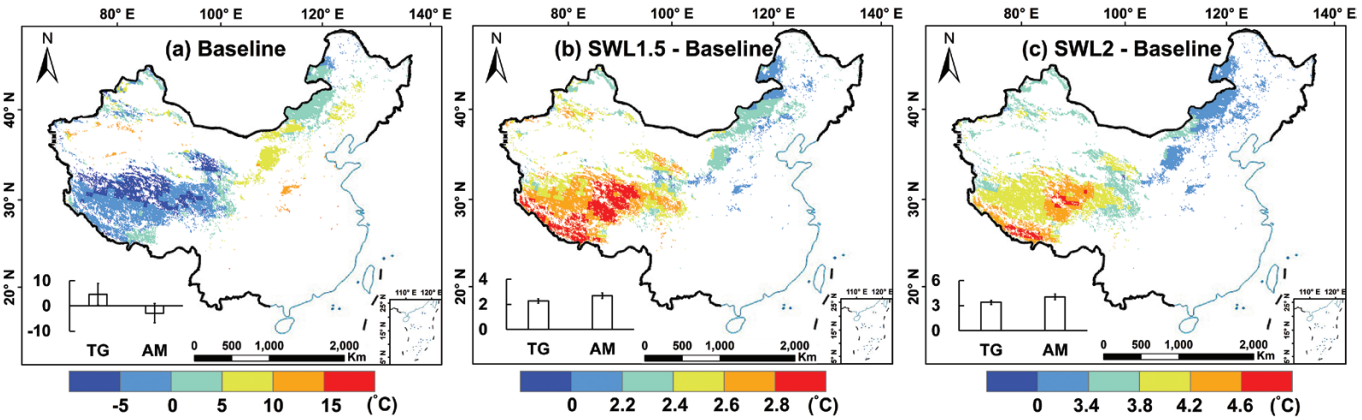

Figure 3: spatial pattern of temperature in Chinese grasslands under baseline (1971–2005) (**a**) and its changes under SWL1.5 (**b**) and SWL2 (**c**). The lower left inset denotes the temperature changes (°C) in temperate grasslands (TG) and alpine meadow (AM).

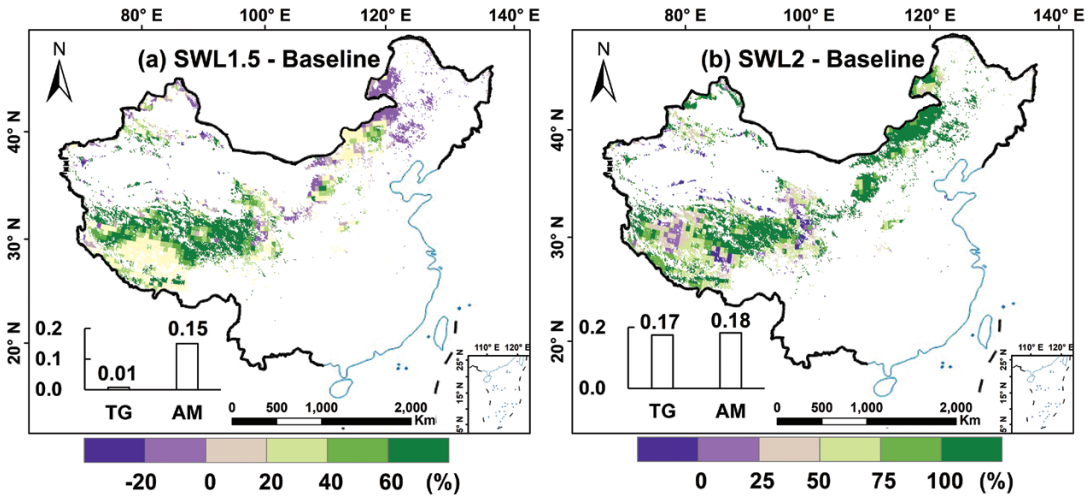

Figure 4: spatial pattern of relative changes in GPP_{MA} from baseline (1971–2005) to SWL1.5 (**a**) and SWL2 (**b**). The lower left inset denotes the changes in GPP_{MA} (Pg C $year^{-1}$) in temperate grasslands (TG) and alpine meadow (AM).

Compared with baseline, 95% of the Chinese grasslands show an increase in GPP_{MA} under SWL2 (Fig. 4b). The total GPP_{MA} of Chinese grasslands increased to 1.17 ± 0.09 Pg C $year^{-1}$ under SWL2 (nearly 1.4 times of baseline), with TG and AM accounting for 42.6% and 57.4%, respectively. The GPP_{MA} of TG and AM during SWL2 increased by 0.17 Pg C $year^{-1}$ (53.73% of the GPP_{MA} in TG under baseline) and 0.18 Pg C $year^{-1}$ (36.94% of the GPP_{MA} in AM under baseline) above baseline (lower left inset in Fig. 4b). Notably, the GPP_{MA} of TG increased by 0.17 Pg C $year^{-1}$ (50.44% of the GPP_{MA} in TG under SWL1.5) between SWL1.5 and SWL2, much larger than the GPP_{MA} increase over AM (0.03 Pg C $year^{-1}$, only 4.82% of the GPP_{MA} in AM under SWL1.5) between the two periods.

Changes in C storage under SWL1.5 and SWL2

The changes in C storage (ΔC storage, expressed as the difference in C storage between baseline and SWLs) exhibited an increase between baseline and SWLs (Fig. 5). The ΔC storage was estimated at 0.64 Pg C and 1.37 Pg C from baseline to SWL1.5 and SWL2, respectively. The ΔC storage increased dramatically in most areas of the AM under SWL1.5 (Fig. 5a), while the TG shown a negative ΔC storage. Accordingly, the ΔC storage of AM and TG between baseline and SWL1.5 was estimated at 0.93 Pg C and −0.29 Pg C, respectively (lower left inset in Fig. 5a). Under SWL2, strong positive ΔC storage was found in the northeastern TG, the middle and southwestern AM (Fig. 5b), and most of these regions had a ΔC storage over 0.4 kg C m^{-2}. Compared with baseline, the ΔC storage could reach 0.70 Pg C in AM, slightly higher than that in TG (0.67 Pg C) under SWL2 (lower left inset in Fig. 5b). Compared with SWL1.5, the total ΔC storage increased by 0.73 Pg C under SWL2. The increased ΔC storage was entirely contributed by TG (0.96 Pg C), whereas the ΔC storage of AM even decreased by 0.23 Pg C from SWL1.5 to SWL2, it somehow

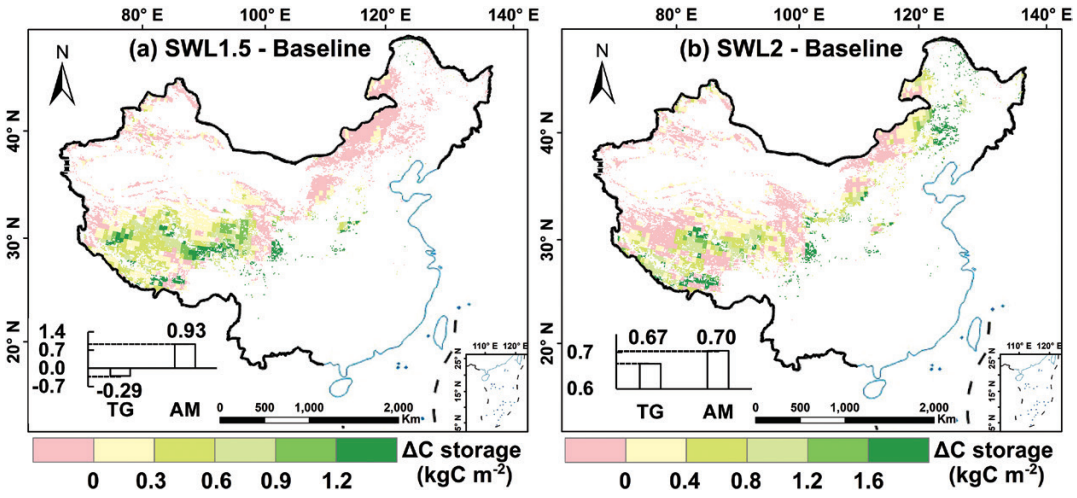

Figure 5: spatial pattern of ΔC storage from baseline (1971–2005) to SWL1.5 (**a**) and SWL2 (**b**). The lower left inset denotes the ΔC storage (Pg C) in temperate grasslands (TG) and alpine meadow (AM).

indicated that the C sequestration potential of TG would be higher than that of AM under SWL2.

Differences in the changes of GPP and C storage between SWLs and RCPs

The ΔGPP_{MA} of the four CMIP5 ESMs exhibited increase from RCP2.6 to RCP8.5 (Fig. 6a), which might attribute to higher CO_2 fertilization in RCP8.5 than that in other scenarios (Anav *et al.* 2015; Friedlingstein *et al.* 2014; Wang *et al.* 2014a). The ΔGPP_{MA} of SWL2 was slightly higher than that of RCP2.6, and close to RCP4.5, while SWL1.5 gains the least ΔGPP_{MA} in all scenarios. The ΔGPP_{MA} of RCP4.5, RCP6.0 and RCP8.5 were 11.9%, 33.4% and 112.9% higher than that of SWL2, respectively. The ΔC storage of Chinses grasslands simulated by the four ESMs ranged from 1.72 Pg C (RCP2.6) to 3.74 Pg C (RCP8.5), which was higher than that under SWLs. SWL1.5 gains the least ΔC storage (0.64 Pg C) of all scenarios, the ΔC storage of SWL2 was close to that of RCP2.6 (1.37 Pg C vs. 1.72 Pg C) (Fig. 6b). In summary, the Chinese grasslands play a role of C sink both in the RCP and SWL scenarios.

Uncertainties of simulated GPP and NBP

For the baseline, we compared the GPP_{MA} and NBP_{MA} of Chinese grasslands modeled by our model to which modeled by the four CMIP5 ESMs in the baseline. The GPP_{MA} of Chinese grasslands, modeled by the ESMs, was ranged from 0.39 Pg C $year^{-1}$ (HadGEM2-ES) to 0.88 Pg C $year^{-1}$ (GFDL-ESM2M) in the baseline (Fig. 7a). The GPP_{MA} of our model (0.82 Pg $year^{-1}$) is greater than that of HadGEM2-ES (0.39 Pg $year^{-1}$), NorESM1-ME (0.68 Pg yr^{-1}) and IPSL-CM5A-LR (0.74 Pg yr^{-1}), but less than that of GFDL-ESM2M (0.88 Pg $year^{-1}$). The NBP of our model indicated a weak C source (−3.61 Tg C $year^{-1}$) in Chinese grasslands during the baseline period, which is close to the simulation of NorESM1-ME (−3.32 Tg C $year^{-1}$). The consistent result was also obtained

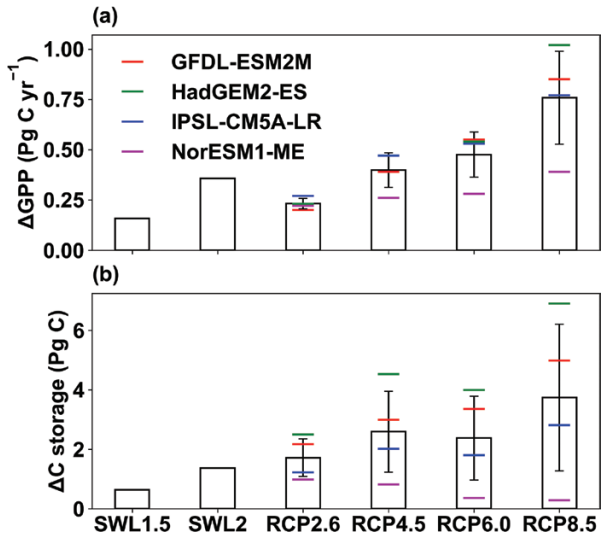

Figure 6: changes in GPP_{MA} (ΔGPP_{MA}) (**a**) and NBP (ΔC storage) (**b**) under SWLs and RCPs in the grasslands of China. ΔGPP_{MA} and ΔC storage of RCPs were calculated as the difference between the GPP_{MA} of last two decades (2081–2100) and that of baseline (1971–2005). Each RCP bar denotes the average ΔGPP_{MA} and ΔC storage of the four CMIP5 ESMs (ΔGPP_{MA} and ΔC storage for each model are marked with horizontal color line).

from GFDL-ESM2M (−34.98 Tg C $year^{-1}$) and HadGEM2-ES (−40.37 Tg C $year^{-1}$), but the C loses nearly 10 times than our model predicted (Fig. 7b). In summary, the GPP_{MA} of Chinese

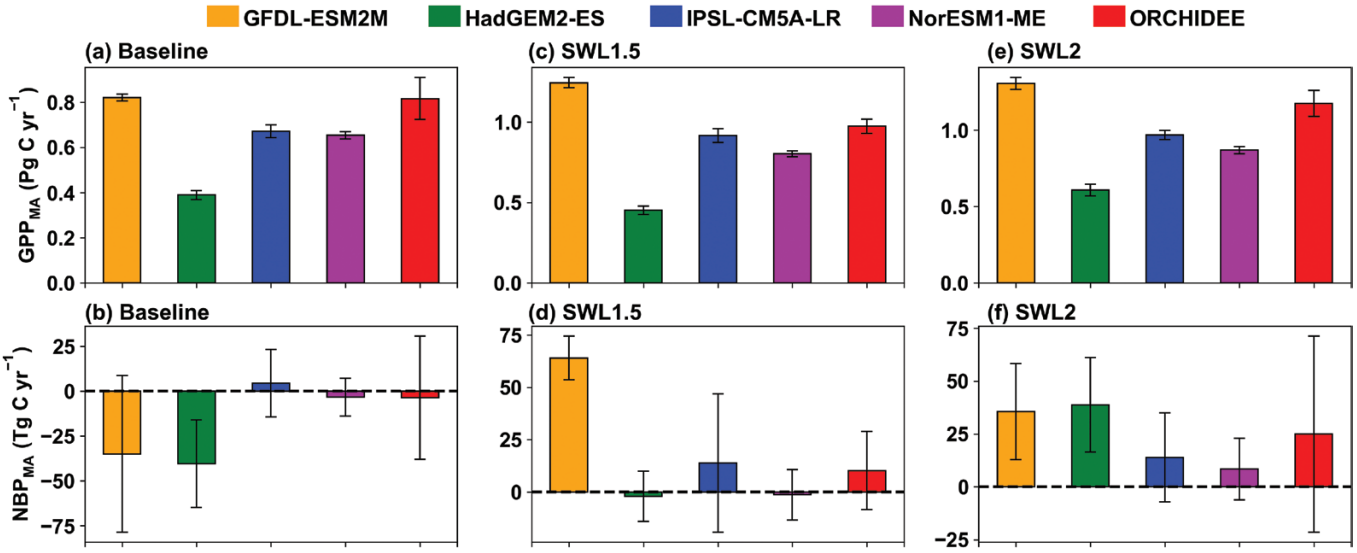

Figure 7: GPP_{MA} (**a**, **c** and **e**) and NBP_{MA} (**b**, **d** and **f**) of Chinese grasslands under baseline and SWLs. The left, middle and right panels show the results of baseline, SWL1.5 and SWL2, respectively. The GPP_{MA} and NBP_{MA} of each CMIP5 ESM were calculated during the 5 years when the temperature reached SWL1.5 and SWL2 (Table 2).

Table 3: comparison of GPP_{MA} of Chinese grasslands between this study and previous estimates

Model/datasets	GPP_{MA} (PgC $year^{-1}$)	Area (km^2)	Period	This study (PgC $year^{-1}$)	Reference
EC-LUE	0.88	2314600	2000–2009	0.84	Li *et al.* (2013)
VPM	0.83	2748492	2006–2008	0.87	Chen *et al.* (2014)
BEPS	0.71	2915546	2001	0.82	Feng *et al.* (2007)

grasslands was around 0.70 ± 0.17 Pg C $year^{-1}$ simulated by multimodel in the baseline, and the result of our model was within the range.

For the future, we compared the GPP and NBP of our model with that of the four CMIP5 ESMs under SWL1.5 and SWL2. The year of each ESM reached SWL1.5 and SWL2 under RCP8.5 was shown in Table 2. We used the GPP_{MA} and NBP_{MA} of 5 years when the temperature was reaching SWL1.5 and SWL2 (e.g. 2034–2038 of GFDL-ESM2M for SWL1.5) to avoid the oscillation induced by extreme values across time series. The GPP_{MA} and NBP_{MA} of our model under SWL1.5 were compared with that of the four ESMs under RCP8.5 at the same warming level (Fig. 7c and d). Our simulated GPP_{MA} of Chinese grasslands was 0.97 Pg C $year^{-1}$ under SWL1.5, close to the result of IPSL-CM5A-LR (0.92 Pg C $year^{-1}$), but higher than that of NorESM1-ME (0.80 Pg C $year^{-1}$) and HadGEM2-ES (0.45 Pg C $year^{-1}$). The NBP_{MA} of GFDL-ESM2M (64.03 Tg C $year^{-1}$) and IPSL-CM5A-LR (13.91 Tg C $year^{-1}$) is consistent with our results (10.29 Tg C $year^{-1}$) that Chinese grasslands play as a role of C sink under SWL1.5. However, HadGEM2-ES (−2.03 Tg C $year^{-1}$) and NorESM1-ME (−1.32 Tg C $year^{-1}$) indicated weak C source in the Chinese grasslands under SWL1.5.

The GPP_{MA} of the four ESMs was ranged from 0.61 (HadGEM2-ES) to 1.30 Pg C $year^{-1}$ (GFDL-ESM2M) when the temperature reached SWL2 (Fig. 7e). The GPP_{MA} of this study was slightly lower than that of GFDL-ESM2M, but higher than the others. The NBP_{MA} of the four ESMs range from 8.38 Tg C $year^{-1}$ (NorESM1-ME) to 38.77 Tg C $year^{-1}$ (HadGEM2-ES) (Fig. 7f), which suggested that the Chinese grasslands were C sink when the temperature reached SLW2. Our simulated NBP_{MA} was 24.93 Tg C $year^{-1}$ under SWL2, which was higher than the results of NorESM1-ME and IPSL-CM5A-LR, but less than that of GFDL-ESM2M and HadGEM2-ES.

DISCUSSION

GPP in Chinese grasslands

We gathered the estimates of GPP in this study and those of earlier studies (Table 3). The results shown that the GPP_{MA} of Chinese grasslands was 0.84 Pg C $year^{-1}$ from 2000 to 2009, less than the estimation of Li *et al.* (2013). In contrast, the GPP_{MA} in this study is higher than that of Chen *et al.* (2014) (from 2006 to 2008) and Feng *et al.* (2007) (in 2001). By comparing with observation-based GPP, our results were thus slightly higher than the GPP_{MA} of FLUXCOM datasets (0.730.93 0.55 (meanmax min) Pg C $year^{-1}$ from 1980 to

2013. The GPP_{MA} of MOD17C6 (0.59 Pg C $year^{-1}$) was much lower than that simulated in this study, and underestimation in GPP of MOD17C6 product is suggested by a recent study (Zhang *et al.* 2017).

Impacts of the changes in GPP and C storage under SWLs and RCPs

The Paris Agreement marks a change in the global climate governance model. Unlike the RCPs that had large uncertainties (from RCP2.6 to RCP8.5) in the future projections, we can now analyze the impacts for the increase in mean annual temperature of 2°C or 1.5°C. The discrepancy of ΔGPP_{MA} in SLWs and RCPs indicated that higher CO_2 fertilization effect (CO_2 concentration reach 1370 ppm in RCP8.5 and 448.8 ppm in SWL2) and a higher temperature for plant photosynthesis could benefit the GPP of AM, while a higher temperature may dampen the GPP of TG. Assuming one sheep unit consumes 2 kg of dry organic matter per day (Chen *et al.* 2008), and 48% of the pasture can be used by livestock (Li 2000; Wang *et al.* 2010), then the ΔGPP_{MA} in RCP8.5 could sustain 52 and 75 million more sheep units per year than SWL2 and SWL1.5, respectively. However, SWL1.5 will greatly reduce the risk from climate extremes which will be a benefit to the livestock industry and human society (Li *et al.* 2018), as well as shrinkage of glacier ice (Kraaijenbrink *et al.* 2017). The ΔC storage presents an increasing trend from SLW1.5 to RCP8.5, which indicate that the Chinese grasslands play a role of C sink under both SWLs and RCPs scenarios, and this will help to mitigate climate warming. The full impacts of SWL1.5 and SWL2 on the sustainable development of Chinese grasslands need further synthesized assessments considering both productivities of grasslands, impacts of extreme climate events and other impacts on grasslands ecosystems.

Potential drivers on the changes in productivity and C storage of grasslands

Compared with baseline, strong increases in GPP and C storage of Chinese grasslands are simulated by using the ORCHIDEE model under SWLs. First, the effect of rising CO_2 concentration is likely to be an important driver. Previous studies found that elevated CO_2 concentration will enhance plant photosynthesis (Drake *et al.* 1997; Poorter 1993) and water use efficiency (Keenan *et al.* 2013). Second, the increases in precipitation, projected under SWLs in most Chinese grasslands, will supply more water for the growth of grasslands, and relieve the drought caused by the rising temperature. Finally, the coupling of increasing CO_2 concentration, temperature and precipitation will extend the vegetation growing season (Piao *et al.* 2007b; Reyes-Fox *et al.* 2014). All these mentioned above might be the main reasons for the larger GPP and C storage of SWLs than that of baseline.

The grassland types have different responses to future climate change. It is generally acknowledged that TG is considered more sensitive to water limitations (Peng *et al.* 2013; Poulter *et al.* 2013), whereas temperature is the dominated climate factor to control C fluxes in AM (Kato *et al.* 2006; Lin *et al.* 2011). The Chinese grassland will become warmer and wetter than baseline under SWL1.5 and SWL2. One of the possible reasons is that global warming accelerates water cycle (Shi *et al.* 2003). The water vapor transport from the Arabian Sea to northwestern China is enhanced because of increase in seawater evaporation driven by the increase in sea temperature in the South Indian Ocean (Shi *et al.* 2003). Another possible reason is likely due to the melting of glaciers leads to an increase in river runoff, which in turn causes an increase in precipitation (Shi *et al.* 2003), although this mechanism is not represented in our model. Overall, the total amount of GPP and ΔC storage was shown an increasing trend from baseline to SWL2. However, changes in precipitation in the Chinese grasslands have considerable spatial heterogeneity, especially in the northeastern IMP, where the precipitation increased marginally or even decreased under SWL1.5. Therefore, drought may offset the CO_2 fertilization effect in the northeastern IMP, and results in a relatively lower increase in GPP and C storage of TG under SWL1.5.

Uncertainties in the C cycle simulation

The GPP and NBP simulated in this study within the range of the four CMIP5 ESMs under baseline, SWL1.5 and SWL2. The uncertainties in the projection of C cycle between our model and ESMs might be attributed to the following aspects. First, the predicted climate between models have large uncertainty, which could be propagated into C cycle simulation. Second, the model structure and parameters can contribute to large uncertainty to the result of the model (Verbeeck *et al.* 2006). The four ESMs have similar photosynthesis algorithm, thus the differences of GPP between our model and ESMs are likely due to parameters settings in the models. Besides, the turnover of C pools is quite different among CMIP5 ESMs (Todd-Brown *et al.* 2013). Third, the interactions between C and nitrogen (N) were not considered in this study. In fact, the changes in C fluxes are strongly affected by soil N availability (Liu *et al.* 2010; Ryals *et al.* 2014; Siemann *et al.* 2003), especially in alpine, arid and semiarid areas where N is the limiting nutrient (Liu *et al.* 2010). The N limitation and deposition effects on C cycle processes would induce further uncertainty of our prediction (Bai *et al.* 2008; Janssens *et al.* 2010; Wang *et al.* 2017b). Fourth, vegetation dynamics, grasslands managements and land cover change are other challenges in C cycle simulation (Piao *et al.* 2018). In our simulations, the grassland types and area in each grid are fixed throughout the simulation. This may underestimate the impacts of disturbances and managements (Chang *et al.* 2017) and overestimate the carbon storage. Finally, the positive effect of CO_2 fertilization on vegetation growth is uncertain (Girardin *et al.* 2016; Sleen *et al.* 2015; Wang *et al.* 2014b). In fact, the effect of CO_2 fertilization, as well as N limitation (Bonan *et al.* 2010; Zaehle *et al.* 2010), is reduced under extreme weather conditions in temperate grasslands (Obermeier *et al.* 2016). Consequently, the current models might overestimate the future C sink of temperate grasslands. In the future, coupled C–N and validated CO_2 fertilization in ESMs could further help predict productivity and potential C sink in grasslands under warming scenarios.

CONCLUSION

This study simulated the GPP and NBP of Chinese grasslands by using the ORCHIDEE model under global warming of 1.5°C and 2°C scenarios. Our results indicated that the grasslands in China would be warmer by 2.5°C and 3.7°C under SWL1.5 and SWL2 than the baseline period. The GPP_{MA} increased by 0.16 and 0.36 Pg C $year^{-1}$, and the C storage increased by 0.64 Pg C and 1.37 Pg C under SWL1.5 and SWL2, respectively. The results of this study hint the increase in productivity and C storage of Chinese grasslands under future global warming, and the C sequestration potential of TG will be more than that of AM under SWL2. Precipitation has a strong effect on the increases in GPP and C storage in Chinese grasslands. Thus, accurate prediction of the future precipitation is critical to the C cycle in Chinese grasslands. In the future, grassland managements, interactions between livestock and grasslands (Chang *et al.* 2017), coupled C–N (Zaehle *et al.* 2010) and impacts of extreme climate events on grasslands (Obermeier *et al.* 2016) should be added in integrated assessment models for further synthesized assessments of the sustainable development of Chinese grasslands.

SUPPLEMENTARY MATERIAL

Supplementary material is available at *Journal of Plant Ecology* online.

FUNDING

This study was supported by the National Key Research and Development Program of China (grant no. 2016YFA0600202 and 2016YFC0500203) and National Basic Research Program of China (grant no. 2013CB956303).

ACKNOWLEDGEMENTS

The MOD17A2H version 6 Gross Primary Productivity (GPP) product from 2001 to 2017 was retrieved from https://lpdaac.usgs.gov, maintained by the NASA EOSDIS Land Processes Distributed Active Archive Center (LP DAAC) at the USGS/Earth Resources Observation and Science (EROS) Center, Sioux Falls, South Dakota. J.C acknowledged support from the European Union Seventh Framework Programme FP7/2007–2013 under grant agreement n° 603864 (HELIX). We thank Dr. Klaus Wyser for providing the high-resolution climate forcing (EC-EARTH3-HR + IPSL-CM5-LR). We thank Dr. Catherine Morfopoulos and Dr. Pierre Friedlingstein for designing the protocol for HELIX climate impacts.

REFERENCES

Akiyama T, Kawamura K (2007) Grassland degradation in China: methods of monitoring, management and restoration. *Grassl Sci* **53**:1–17.

Alfieri L, Bisselink B, Dottori F, *et al.* (2017) Global projections of river flood risk in a warmer world. *Earth Future* **5**:171–82.

Alfieri L, Feyen L, Di Baldassarre G (2016) Increasing flood risk under climate change: a pan-European assessment of the benefits of four adaptation strategies. *Clim Change* **136**:507–21.

Anav A, Friedlingstein P, Beer C, *et al.* (2015) Spatiotemporal patterns of terrestrial gross primary production: a review. *Rev Geophys* **53**:785–818.

Bai W, Wang Z, Chen Q, *et al.* (2008) Spatial and temporal effects of nitrogen addition on root life span of *Leymus chinensis* in a typical steppe of inner Mongolia. *Funct Ecol* **22**:583–91.

Bonan GB, Levis S (2010) Quantifying carbon-nitrogen feedbacks in the community land model (CLM4). *Geophys Res Lett* **37**:256–65.

Chadburn SE, Burke EJ, Essery RLH, *et al.* (2015) Impact of model developments on present and future simulations of permafrost in a global land-surface model. *Cryosphere* **9**:1505–21.

Chang J, Ciais P, Viovy N, *et al.* (2017) Future productivity and phenology changes in European grasslands for different warming levels: implications for grassland management and carbon balance. *Carbon Balance Manage* **12**:11.

Chen S, Wang S, Yi Z (2008) Estimation of Chinese grassland productivity using remote sensing. *Trans CSAE* **24**:208–12.

Chen J, Yan H, Wang S, *et al.* (2014) Estimation of gross primary productivity in Chinese terrestrial ecosystems by using VPM model. *Quat Sci* **34**:732–42.

Chen H, Zhu Q, Peng C, *et al.* (2013) The impacts of climate change and human activities on biogeochemical cycles on the Qinghai-Tibetan Plateau. *Glob Change Biol* **19**:2940–55.

Conant RT, Paustian K, Elliott ET (2001) Grassland management and conversion into grassland: effects on soil carbon. *Ecol Appl* **11**:343–55.

Drake BG, Gonzalez-Meler MA, Long SP (1997) More efficient plants: a consequence of rising atmospheric CO_2? *Annu Rev Plant Physiol Plant Mol Biol* **48**:609–39.

Feng X, Liu G, Chen JM, *et al.* (2007) Net primary productivity of China's terrestrial ecosystems from a process model driven by remote sensing. *J Environ Manage* **85**:563–73.

Friedlingstein P, Meinshausen M, Arora VK, *et al.* (2014) Uncertainties in CMIP5 climate projections due to carbon cycle feedbacks. *J Climate* **27**:511–26.

Girardin MP, Bouriaud O, Hogg EH, *et al.* (2016) No growth stimulation of Canada's boreal forest under half-century of combined warming and CO_2 fertilization. *Proc Natl Acad Sci USA* **113**:E8406–14.

Hazeleger W, Wang X, Severijns C, *et al.* (2012) EC-Earth V2.2: description and validation of a new seamless earth system prediction model. *Clim Dynam* **39**:2611–29.

He N, Chen Q, Han X, *et al.* (2012) Warming and increased precipitation individually influence soil carbon sequestration of Inner Mongolian grasslands, China. *Agric Ecosyst Environ* **158**:184–91.

Janssens IA, Dieleman W, Luyssaert S, *et al.* (2010) Reduction of forest soil respiration in response to nitrogen deposition. *Nat Geosci* **3**:315–22.

Jin H, Li S, Cheng G, *et al.* (2000) Permafrost and climatic change in China. *Glob Planet Change* **26**:387–404.

Jung M, Reichstein M, Schwalm CR, *et al.* (2017) Compensatory water effects link yearly global land CO_2 sink changes to temperature. *Nature* **541**:516–20.

Kato T, Tang Y, Gu S, *et al.* (2006) Temperature and biomass influences on interannual changes in CO_2 exchange in an alpine meadow on the Qinghai-Tibetan plateau. *Glob Change Biol* **12**:1285–98.

Keenan TF, Hollinger DY, Bohrer G, *et al.* (2013) Increase in forest water-use efficiency as atmospheric carbon dioxide concentrations rise. *Nature* **499**:324–7.

Kraaijenbrink PDA, Bierkens MFP, Lutz AF, *et al.* (2017) Impact of a global temperature rise of 1.5 degrees Celsius on Asia's glaciers. *Nature* **549**:257–60.

Krinner G, Viovy N, Noblet-Ducoudré ND, *et al.* (2005) A dynamic global vegetation model for studies of the coupled atmosphere-biosphere system. *Glob Biogeochem Cycle* **19**:GB1015.

Li Y (2000) Simulation of forage yield and stocking rate on alpine grassland in response to warming trend of climate. *Acta Pratacult Sin* **9**:77–82.

Li X, Liang S, Yu G, *et al.* (2013) Estimation of gross primary production over the terrestrial ecosystems in China. *Ecol Model* **261**:80–92.

Li D, Zhou T, Zou L, *et al.* (2018) Extreme high-temperature events over East Asia in 1.5°C and 2°C warmer futures: analysis of NCAR CESM low-warming experiments. *Geophys Res Lett* **45**:1541–50.

Lin X, Zhang Z, Wang S, *et al.* (2011) Response of ecosystem respiration to warming and grazing during the growing seasons in the alpine meadow on the Tibetan plateau. *Agric For Meteorol* **151**:792–802.

Liu P, Huang J, Sun OJ, *et al.* (2010) Litter decomposition and nutrient release as affected by soil nitrogen availability and litter quality in a semiarid grassland ecosystem. *Oecologia* **162**:771–80.

Lovell R, Jarvis S, Bardgett R (1995) Soil microbial biomass and activity in long-term grassland: effects of management changes. *Soil Biol Biochem* **27**:969–75.

Lu M, Zhou X, Yang Q, *et al.* (2013) Responses of ecosystem carbon cycle to experimental warming: a meta-analysis. *Ecology* **94**:726–38.

Nan Z (2005) The grassland farming system and sustainable agricultural development in China. *Grassl Sci* **51**:15–9.

National Bureau of Statistics of China (2016) *China Statistical Yearbook*. Beijing: China Statistical Publishing House.

Obermeier WA, Lehnert LW, Kammann CI, *et al.* (2016) Reduced CO_2 fertilization effect in temperate C3 grasslands under more extreme weather conditions. *Nat Clim Change* **7**:137–41.

Peng S, Piao S, Shen Z, *et al.* (2013) Precipitation amount, seasonality and frequency regulate carbon cycling of a semi-arid grassland ecosystem in inner Mongolia, China: a modeling analysis. *Agric For Meteorol* **178**:46–55.

Piao S, Ciais P, Friedlingstein P, *et al.* (2009a) Spatiotemporal patterns of terrestrial carbon cycle during the 20th century. *Glob Biogeochem Cycle* **23**:2091–6.

Piao S, Fang J, Ciais P, *et al.* (2009b) The carbon balance of terrestrial ecosystems in China. *Nature* **458**:1009–13.

Piao S, Fang J, Zhou L, *et al.* (2005) Changes in vegetation net primary productivity from 1982 to 1999 in China. *Glob Biogeochem Cycle* **19**:15242–7.

Piao S, Friedlingstein P, Ciais P, *et al.* (2007a) Changes in climate and land use have a larger direct impact than rising CO_2 on global river runoff trends. *Proc Natl Acad Sci USA* **104**:15242–7.

Piao S, Friedlingstein P, Ciais P, *et al.* (2007b) Growing season extension and its impact on terrestrial carbon cycle in the northern hemisphere over the past 2 decades. *Glob Biogeochem Cycle* **21**:1148–54.

Piao S, Huang M, Liu Z, *et al.* (2018) Lower land-use emissions responsible for increased net land carbon sink during the slow warming period. *Nat Geosci* **11**:739–43.

Poorter H (1993) Interspecific variation in the growth response of plants to an elevated ambient CO_2 concentration. *Vegetatio* **104/105**:77–97.

Poulter B, Pederson N, Liu H, *et al.* (2013) Recent trends in inner Asian forest dynamics to temperature and precipitation indicate high sensitivity to climate change. *Agric For Meteorol* **178**:31–45.

Reyes-Fox M, Steltzer H, Trlica MJ, *et al.* (2014) Elevated CO_2 further lengthens growing season under warming conditions. *Nature* **510**:259–62.

Running S, Mu Q, Zhao M (2015) *MOD17A2H MODIS/AQUA gross primary productivity 8-day l4 global 500m sin grid: NASA LP DAAC.* https://lpdaac.usgs.gov/products/mod17a2hv006/

Ryals R, Kaiser M, Torn MS, *et al.* (2014) Impacts of organic matter amendments on carbon and nitrogen dynamics in grassland soils. *Soil Biol Biochem* **68**:52–61.

Schleussner CF, Lissner TK, Fischer EM, *et al.* (2016) Differential climate impacts for policy-relevant limits to global warming: the case of 1.5 °C and 2 °C. *Earth Syst Dynam* **7**:327–51.

Scurlock JMO, Hall DO (1998) The global carbon sink: a grassland perspective. *Global Change Biol* **4**:229–33.

Shi Y, Shen Y, Li D, *et al.* (2003) Discussion on the present climate change from warm-dry to warm-wet in Northwest China. *Quat Sci* **23**:152–64.

Siemann E, Rogers WE (2003) Changes in light and nitrogen availability under pioneer trees may indirectly facilitate tree invasions of grasslands. *J Ecol* **91**:923–31.

Sleen PVD, Groenendijk P, Vlam M, *et al.* (2015) No growth stimulation of tropical trees by 150 years of CO_2 fertilization but water-use efficiency increased. *Nat Geosci* **8**:24–8.

Taylor KE, Stouffer RJ, Meehl GA (2012) An overview of CMIP5 and the experiment design. *Bull Am Meteorol Soc* **93**:485–98.

Todd-Brown KEO, Randerson JT, Post WM, *et al.* (2013) Causes of variation in soil carbon simulations from cmip5 earth system models and comparison with observations. *Biogeosciences* **10**:1717–36.

Tramontana G, Jung M, Schwalm CR, *et al.* (2016) Predicting carbon dioxide and energy fluxes across global FLUXNET sites with regression algorithms. *Biogeosciences* **13**:1–33.

Vautard R, Gobiet A, Sobolowski S, *et al.* (2014) The European climate under a 2 °C global warming. *Environ Res Lett* **9**:034006.

Verbeeck H, Samson R, Verdonck F, *et al.* (2006) Parameter sensitivity and uncertainty of the forest carbon flux model FORUG: a Monte Carlo analysis. *Tree Physiol* **26**:807–17.

Wang G, Cai W, Gan B, *et al.* (2017a) Continued increase of extreme El Niño frequency long after 1.5°C warming stabilization. *Nat Clim Change* **7**:568–72.

Wang Y, Law RM, Pak B (2010) A global model of carbon, nitrogen and phosphorus cycles for the terrestrial biosphere. *Biogeosciences* **7**:2261–82.

Wang T, Lin X, Peng S, *et al.* (2014a) Multi-model projections and uncertainties of net ecosystem production in China over the twenty-first century. *Sci Bull* **59**: 4681–91.

Wang X, Piao S, Ciais P, *et al.* (2014b) A two-fold increase of carbon cycle sensitivity to tropical temperature variations. *Nature* **506**:212–5.

Wang Z, Yang Y, Li J, *et al.* (2017b) Simulation of terrestrial carbon equilibrium state by using a detachable carbon cycle scheme. *Ecol Indic* **75**:82–94.

Wang Z, Zhang Y, Yang Y, *et al.* (2016) Quantitative assess the driving forces on the grassland degradation in the Qinghai–Tibet plateau, in China. *Ecol Inform* **33**:32–44.

Xu Y, Ramanathan V (2017) Well below 2°C: mitigation strategies for avoiding dangerous to catastrophic climate changes. *Proc Natl Acad Sci USA* **114**:10315–23.

Yao Y, Piao S, Wang T (2018) Future biomass carbon sequestration capacity of Chinese forests. *Sci Bull* **63**:1108–17.

Zaehle S, Friend AD, Friedlingstein P, *et al.* (2010) Carbon and nitrogen cycle dynamics in the O-CN land surface model: 2. Role of the nitrogen cycle in the historical terrestrial carbon balance. *Glob Biogeochem Cycle* **24**:1468–70.

Zhang X (2007) *Vegetation of China and Its Geographic Pattern: Illustration of the Vegetation Map of the People's Republic of China (1: 1 000 000)*. Beijing: Geological Publishing House.

Zhang Y, Xiao X, Wu X, *et al.* (2017) A global moderate resolution dataset of gross primary production of vegetation for 2000-2016. *Sci Data* **4**:170165.